PHILOSOPHICAL TRANSACTIONS OF THE ROYAL SOCIETY A MATHEMATICAL, PHYSICAL & ENGINEERING SCIENCES

Current-induced spin–orbit torques

Pietro Gambardella and Ioan Mihai Miron

Phil. Trans. R. Soc. A 2011 **369**, 3175-3197
doi: 10.1098/rsta.2010.0336

PHILOSOPHICAL TRANSACTIONS OF THE ROYAL SOCIETY A

Phil. Trans. R. Soc. A (2011) **369**, 3175–3197
doi:10.1098/rsta.2010.0336

Review

Current-induced spin–orbit torques

By Pietro Gambardella[1,2,*] and Ioan Mihai Miron[1]

[1]*Institut Catalá de Nanotecnologia, Centre d'Investigaciò en Nanociència i Nanotecnologia (ICN-CIN2), UAB Campus, 08193 Barcelona, Spain*
[2]*Institució Catalana de Recerca i Estudis Avançats (ICREA), 08100 Barcelona, Spain*

The ability to reverse the magnetization of nanomagnets by current injection has attracted increased attention ever since the spin-transfer torque mechanism was predicted in 1996. In this paper, we review the basic theoretical and experimental arguments supporting a novel current-induced spin torque mechanism taking place in ferromagnetic (FM) materials. This effect, hereafter named spin–orbit (SO) torque, is produced by the flow of an electric current in a crystalline structure lacking inversion symmetry, which transfers orbital angular momentum from the lattice to the spin system owing to the combined action of SO and exchange coupling. SO torques are found to be prominent in both FM metal and semiconducting systems, allowing for great flexibility in adjusting their orientation and magnitude by proper material engineering. Further directions of research in this field are briefly outlined.

Keywords: spin torque; spin–orbit coupling; Rashba effect; Dresselhaus effect; spintronics

1. Introduction

Methods to manipulate the magnetization of ferromagnets alternative to the external magnetic field open a wide spectrum of opportunities to integrate magnetic functionalities into electronic circuits. In recent years, much effort has been devoted to physical processes that take place either in close proximity to or within the core magnetic element of a device, with the multiple aim of reducing its dimensions and energy consumption and eliminating concerns related to the stray field extension typical of write heads. In the following, we briefly review different approaches to this problem, focusing on the generation of spin–orbit (SO) effective magnetic fields in ferromagnets owing to the combined action of an electric current and an asymmetric crystal field intrinsic to materials lacking inversion symmetry.

The possibility to use a spin-polarized current to induce a local torque on magnetization dates back to the seminal work of Slonczewski [1] and Berger [2], and since then it has been investigated extensively both theoretically and experimentally [3]. The physical principle behind this effect is called spin-transfer torque (STT) and requires the flow of an electric current between non-collinear

*Author for correspondence (pietro.gambardella@icrea.es).

One contribution of 12 to a Theme Issue 'New directions in spintronics'.

magnetic structures to transfer spin angular momentum from one to another. The latter can be realized in two ferromagnetic (FM) layers separated by a non-magnetic metal spacer (spin valve) or insulator (magnetic tunnel junction), as well as in domain walls (DWs). Typical current density values required to induce the switching of one magnetic configuration with respect to the other range around $10^7\,\mathrm{A\,cm^{-2}}$. Despite its great fundamental and practical interest, the exploitation of STT to write information in, for example, magnetic tunnel junctions (MTJs) still suffers from the need to compromise between large current density (requiring low junction resistance to avoid damage) and readability (requiring large magnetoresistance). Moreover, optimization of the spin polarization across the junction, stabilization of the 'fixed' layer magnetization, and minimization of stray fields often result in complex stacking structures involving more than 10 different layers.

Alternative to STT, actuation methods based on the application of static electric fields across a magnetic layer have been demonstrated in gated dilute magnetic semiconductor devices through control of the charge carrier density mediating ferromagnetism [4], as well as multi-ferroic/FM heterostructures through the combined effects of magnetoelectric and exchange coupling [5,6]. Voltage-induced changes of magnetic anisotropy and coercivity have been also evidenced in ultrathin FM metal films owing to charge-induced band-structure modifications [7,8]. These effects have great fundamental and applied interest, but temperature and/or magnitude considerations still limit their practical use to prototype demonstrations.

Very recently, a third way has emerged to control the magnetic state of an FM layer, which we refer to as current-induced *SO torque*. Although it exploits both the flow of a spin-polarized current and static electric fields, such a torque is fundamentally different from the processes described above, relying on the presence of strong SO coupling intrinsic to the nuclear composition and atomic structure of a material. The correlation between charge current and spin polarization arising from the SO interaction has been extensively studied in non-magnetic semiconductors since the 1970s [9–11] and recently reviewed by Ganichev & Prettl [12], Silsbee [13] and Awschalom & Samarth [14]. It is only in the last 2 years, however, that current-induced SO-effective magnetic fields have been predicted to occur in ferromagnets [15–17] and their existence demonstrated in dilute magnetic semiconductors [18] and ultrathin metal films [19]. Such investigations bridge two of the main research areas in spintronics, the one based on magnetic multi-layer devices [20] and the one 'without magnetism' based on the manipulation of the electron spin in non-magnetic conductors [14]. The observation of strong SO torques at room temperature combined with the simple layer structure and robust FM properties of metal films [19] open a promising new avenue to manipulate the magnetization of spintronic devices by means of electric currents.

This paper is organized as follows. In §2 we review the spin-splitting of the conduction states in non-magnetic materials lacking inversion symmetry, resulting in the coupling of electron wavevector and spin mediated by the SO interaction. Relevant examples and material issues are discussed for the Rashba and linear Dresselhaus Hamiltonians. In §3, we show how SO coupling induces a net spin polarization of the conduction electrons in the presence of an electric current, analogously to a wavevector-dependent magnetic field. The joint action

of SO and exchange interactions in FM materials is discussed in §4*a*, where SO torques are introduced and compared with STT (§4*b*). Finally, we review the experimental evidence and quantitative measurements of SO torques in dilute magnetic semiconductors (§4*c*) and FM metal films (§4*d*), comparing the two cases and discussing other experiments in light of recent progress in this field.

2. Spin–orbit coupling in materials lacking inversion symmetry

Time-reversal symmetry and inversion symmetry in a crystal structure require that the energy eigenvalues of the electron states satisfy the relationship $E_{\uparrow\downarrow,\mathbf{k}} = E_{\downarrow\uparrow,\mathbf{k}}$, where $\downarrow\uparrow$ denotes up/down spin and $\mathbf{k}$ the electron wavevector. This is the usual spin degeneracy of single electron states in the absence of external or internal magnetic fields. In the absence of inversion symmetry, however, only $E_{\uparrow\downarrow,\mathbf{k}} = E_{\downarrow\uparrow,-\mathbf{k}}$ needs to be satisfied, leading to a $\mathbf{k}$-dependent spin-splitting of the electron bands [21]. Although in non-magnetic materials the number of occupied spin-up and spin-down states at equilibrium is equal, such a correlation between electron wavevector and spin can lead to a net out-of-equilibrium spin polarization in the presence of an electric current.

Dresselhaus [22] has shown that bulk inversion asymmetry (BIA) in non-centrosymmetric crystals with zinc blende structure leads to spin splitting both linear and cubic in k for the heavy/light hole and conduction bands, respectively. Symmetry reduction owing to uniaxial strain allows SO terms linear in k to appear as well in the conduction band [23]. Moreover, Rashba [24] has shown that a crystal with a single high-symmetry axis and an invariant vector oriented along this axis also lead to spin splitting linear in k. The latter situation is realized in wurtzite-type crystals [24,25] as well as in layered heterostructures [26,27], which present structure inversion asymmetry (SIA) along the surface normal. As this review focuses on SO torques in thin films, it is convenient to summarize different forms of the SO Hamiltonian that include both linear SIA and BIA effects for electrons confined in the plane of (100), (110) and (111) layers with zinc blende structure. Following Cartoixà *et al.* [28] and Matos-Abiague & Fabian [17], one has

$$\text{(100) layers:}\quad \mathcal{H}_{\mathrm{SO}} = \alpha(k_y\sigma_x - k_x\sigma_y) + \gamma(k_x\sigma_x - k_y\sigma_y), \tag{2.1}$$

$$\text{(110) layers:}\quad \mathcal{H}_{\mathrm{SO}} = \alpha k_y\sigma_x + \beta k_x\sigma_y + \lambda k_x\sigma_z \tag{2.2}$$

and

$$\text{(111) layers:}\quad \mathcal{H}_{\mathrm{SO}} = (\alpha+\gamma)(k_y\sigma_x - k_x\sigma_y). \tag{2.3}$$

Here, α, γ, β and λ denote material-dependent constants that scale with the strength of the SO interaction (table 1), and $\sigma_{x,y,z}$ are the usual Pauli matrices for the spin. The notation is such that $\hat{\mathbf{x}} \parallel [100]$, $\hat{\mathbf{y}} \parallel [110]$ for a (100) layer, $\hat{\mathbf{x}} \parallel [1\bar{1}0]$, $\hat{\mathbf{y}} \parallel [001]$ for a (110) layer and $\hat{\mathbf{x}} \parallel [11\bar{2}]$, $\hat{\mathbf{y}} \parallel [\bar{1}10]$ for a (111) layer. Note that other works use a rotated reference frame that leads to formally different expressions for $\mathcal{H}_{\mathrm{SO}}$ [12]. Equations (2.1)–(2.3) are relevant not only for quantum well structures in zinc blende semiconductors [21,29,30], but also for (Ga,Mn)As films [18] and metal/semiconductor layers such as Fe/GaAs [31]. In the case of metal surfaces [32,33] and metal layers deposited between asymmetric cubic and amorphous

Table 1. Values of the Rashba and linear Dresselhaus SO constants (α, γ) for semiconducting and metallic systems, energy difference between the SO-split subbands at the Fermi level $\Delta\varepsilon = \varepsilon_{+,k_{F+}} - \varepsilon_{+,k_{F-}}$, saturation magnetization $(\mu_0 M_s)$ and SO torque efficiency in FM systems (B_{SO}/j).

system	α (eV Å)	γ (eV Å)	$\Delta\varepsilon$ (me V)	$\mu_0 M_s$ (T)	B_{SO}/j (T cm^2 A^{-1})
GaAs(001)/AlGaAs[a]	0.07	n.d.	1.4	0	—
InGaAs(001)/InAlAs[b]	0.06–0.1	n.d.	5–6	0	—
GaAs(001)/InGaAs[c]	0.0015	0.0014	n.d.	0	—
Au(111)[d,e]	0.33	0	110	0	—
Ag(111)[e,f]	0.04[g]	0	$\lesssim 2$[g]	0	—
Ag(111)/Bi($\sqrt{3}\times\sqrt{3}$)$R30°$[h]	3.05	0	—	0	—
Gd(0001)[i,j]	0.05[g]	0	15	2.4	—
Gd(0001)/O$p(1\times1)$[i]	0.25[g]	0	100	n.d.	—
GaAs(001)/$Ga_{1-x}Mn_xAs$[k]	0	0.002	n.d.	$\lesssim 0.1$[g]	$2\text{–}5\times10^{-10}$
Pt(poly)/Co/AlO_x[l]	1[g]	0	n.d.	1.37	1×10^{-8}

[a]Stormer *et al.* [35].
[b]Nitta *et al.* [36].
[c]Meier *et al.* [30].
[d]LaShell *et al.* [32].
[e]Cercellier *et al.* [37].
[f]Popović *et al.* [38].
[g]Estimated.
[h]Ast *et al.* [39].
[i]Krupin *et al.* [34].
[j]Elliott *et al.* [40].
[k]Chernyshov *et al.* [18].
[l]Miron *et al.* [19].

interfaces [19,34], $\gamma = \beta = \lambda = 0$, i.e. only the Rashba interaction survives. The latter can be written in vector form as

$$\mathcal{H}_{SO} = \alpha(\mathbf{k} \times \hat{\mathbf{z}}) \cdot \boldsymbol{\sigma}, \tag{2.4}$$

where $\boldsymbol{\sigma} = (\sigma_x, \sigma_y, \sigma_z)$ and $\hat{\mathbf{z}}$ is a unitary vector perpendicular to the layer surface.

Equations (2.1)–(2.3) formally correspond to the interaction of an effective **k**-dependent magnetic field with the electron spin; this can be seen by writing the SO Hamiltonian as

$$\mathcal{H}_{SO} = -\mathbf{m} \cdot \mathbf{B}_{SO} = \mu_B \boldsymbol{\sigma} \cdot \mathbf{B}_{SO}, \tag{2.5}$$

where $m = -g\mu_B \mathbf{s} \approx -\mu_B \boldsymbol{\sigma}$ is the electron magnetic moment operator, **s** the spin, and $\mu_B = e\hbar/(2m_e)$. The orientation of $\mathbf{B}_{SO}(\mathbf{k})$ in four particular cases is shown in figure 1. Note that, in the presence of an external magnetic field [41] or exchange splitting [34,42,43], both time-reversal and inversion symmetry may be broken, leading to a more complex relationship between **k** and spin depending on the relative strength of the SO relative to exchange splitting (§4*a*). In real two-dimensional systems, the point-group symmetry of the surface lattice and the presence of in-plane electric field gradients between dissimilar atomic species may further lead to out-of-plane components of the **k**-dependent spin polarization [39,44].

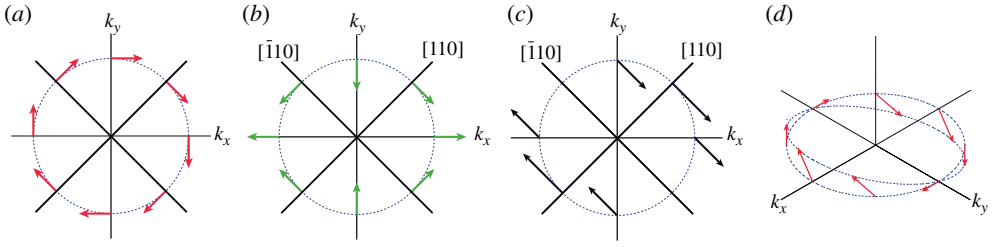

Figure 1. Orientation of the SO-induced magnetic field (arrows) as a function of current direction (solid lines). (*a*) Rashba field originating from the Hamiltonian (2.1) with $\gamma = 0$, or, equivalently, from equation (2.3). (*b*) Linear Dresselhaus field from equation (2.1) with $\alpha = 0$. (*c*) Coexisting Rashba and Dresselhaus fields in equation (2.1) for the special case $\alpha = \gamma$. (*d*) Field corresponding to equation (2.2) for $\alpha = \lambda = -\beta$. (Online version in colour.)

It is easy to understand how either BIA or SIA result in magnetic field-like interactions by considering the motion of electrons in an asymmetric crystal field potential (V). At non-relativistic speed (v), the net electric field originating from such a potential $\mathbf{E} = -\boldsymbol{\nabla} V$ transforms into a magnetic field $-(\mathbf{v} \times \mathbf{E})/c^2$ in the electron's rest frame. When transforming back into the laboratory's reference frame, the magnetic induction field experienced by the electron is corrected by a factor 2, giving $\mathbf{B}_{\mathrm{SO}} = -(\mathbf{v} \times \mathbf{E})/(2c^2) = (\hbar \mathbf{k} \times \boldsymbol{\nabla} V)/(2m_{\mathrm{e}}c^2)$ [45]. The SO Hamiltonian is then given by $-\mathbf{m} \cdot \mathbf{B}_{\mathrm{SO}}$. One shall notice that, in the case of SIA, the conduction electrons feel at the same time the electrostatic potential of the nuclear charge, V_{nuc}, as well as the 'macroscopic' interface potential, V_{int}. This is because the electron wave function can be decomposed into the sum of quickly oscillating lattice-periodic Bloch waves times an envelope function, which feel the microscopic electric field from the atomic cores and the macroscopic field of the SIA environment, respectively [21]. The SO Hamiltonian can then be written as the sum of two terms [46]:

$$\mathcal{H}_{\mathrm{SO}} = \frac{e\hbar^2}{4m_{\mathrm{e}}c^2}\boldsymbol{\sigma} \cdot [\mathbf{k} \times \boldsymbol{\nabla}(V_{\mathrm{nuc}} + V_{\mathrm{int}})]. \tag{2.6}$$

A simple tight-binding model shows that the effective Rashba constant α is proportional to the product of the atomic SO parameter times the hopping matrix element between orbitals with in-plane and out-of-plane symmetry, representing the interface potential gradient [47]. In BIA crystals, on the other hand, only the nuclear term survives. In the central field approximation, one has $V_{\mathrm{nuc}}(r) \approx Ze/(4\pi\varepsilon_0 r)$, where Z denotes the atomic charge, r the distance from the nucleus and ε_0 the vacuum permittivity. Calculating the gradient $\boldsymbol{\nabla} V = (\vec{r}/r)(\mathrm{d}V(r)/\mathrm{d}r) = -(Ze/4\pi\varepsilon_0)(\vec{r}/r^3)$ gives the SO interaction term familiar from atomic physics

$$\mathcal{H}_{\mathrm{nuc}}^{\mathrm{SO}} = \frac{Ze^2\hbar^2}{8\pi\varepsilon_0 m_{\mathrm{e}}^2 c^2 r^3}\frac{\boldsymbol{\sigma}}{2} \cdot \mathbf{l} = \xi(r)\frac{\boldsymbol{\sigma}}{2} \cdot \mathbf{l}, \tag{2.7}$$

where $\hbar\mathbf{l} = (\mathbf{r} \times \hbar\mathbf{k})$ is the orbital angular momentum of the electron, and $\xi = \langle \xi(r) \rangle$ the SO parameter of the shell to which the electron belongs.

By including the Z-dependence of the average $1/r^3$ contribution in equation (2.5), one has $\xi \sim Z^4$, which explains the need to include heavy atoms to obtain sizeable Rashba or Dresselhaus coupling constants.

3. Current-induced spin polarization

SO coupling has well-known consequences on the transport properties of both magnetic and non-magnetic conductors, contributing to the anisotropic magnetoresistance [48], anomalous Hall effect (AHE) [49,50], and extrinsic [9,51] and intrinsic [52] spin Hall effect. These phenomena originate from asymmetric scattering from impurities as well as intrinsic band-structure properties [50]. Both the anomalous and spin Hall effects create spin accumulation of opposite sign localized at the edges of the conductor. In contrast to such spatially non-uniform phenomena, several authors have pointed out the possibility to induce a homogeneous net spin polarization by passing an electric current through non-magnetic semiconductors lacking inversion symmetry [10,11,53–55]. This type of spin accumulation is due to the uneven occupation of k and −k states in the presence of a charge current, which produces a non-zero average effective field acting on the spin density of the conduction electrons, with the symmetry described in §2. Such phenomenon is also described as an inverse spin galvanic effect, which has been experimentally detected in strained bulk semiconductors [51,56] and heterogeneous quantum well structures [57,58]. The conduction electron spin-polarization mechanism turns out to be critical for the generation of SO torques in magnetic materials [15,16,59] and shall therefore be analysed in some detail. For simplicity, we follow here a simple model for a non-magnetic SIA conductor presented by Silsbee [60], which can then be extended, at least qualitatively, to the case of an FM conductor. Keeping into account the Rashba SO interaction of equation (2.4), the total Hamiltonian of a two-dimensional electron gas is

$$\mathcal{H} = \frac{\hbar^2 k^2}{2m_{\mathrm{e}}^*} + \alpha(\mathbf{k} \times \hat{\mathbf{z}}) \cdot \boldsymbol{\sigma}, \tag{3.1}$$

where m_{e}^* represents the effective electron mass. Straightforward diagonalization of this Hamiltonian gives the eigenvalues

$$\varepsilon_{\pm,\mathbf{k}} = \frac{\hbar^2 k^2}{2m_{\mathrm{e}}^*} \pm \alpha|k| \tag{3.2}$$

and eigenvectors

$$\psi_{\pm,\mathbf{k}} = \frac{\mathrm{e}^{\mathrm{i}\mathbf{k}\cdot\mathbf{r}}}{\sqrt{2A}} \begin{pmatrix} 1 \\ \mp \mathrm{i}\mathrm{e}^{\mathrm{i}\xi_{\mathbf{k}}} \end{pmatrix}, \tag{3.3}$$

where $\mathbf{k} = k(\cos\xi, \sin\xi, 0)$ and A is the area of the layer. The coupling between orbital and spin degrees of freedom is evident from the spinor expression in equation (3.3), and is also a general feature of more realistic models that use Bloch states to describe the electronic states in a periodic lattice. The spin expectation

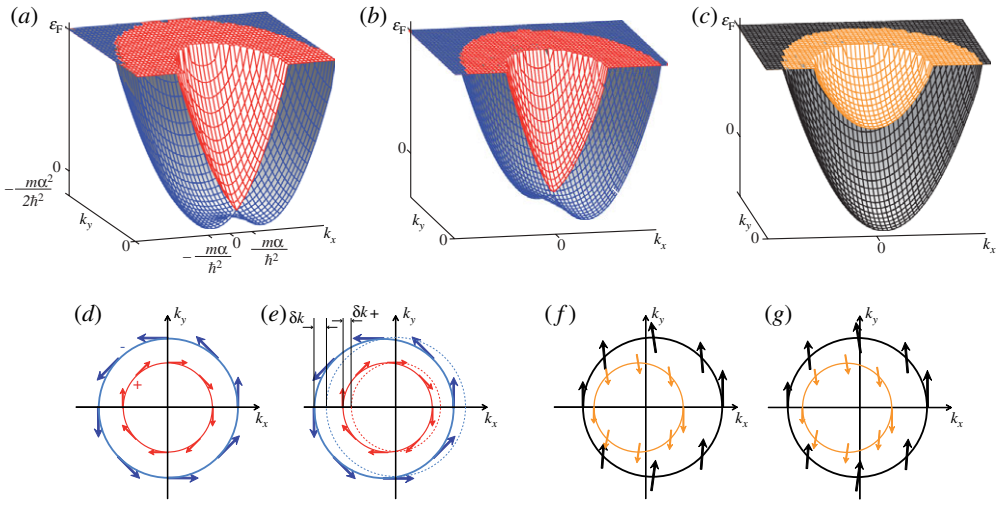

Figure 2. Two-dimensional energy dispersion $\varepsilon_{\pm,\mathbf{k}}$ of a Rashba system calculated from equation (4.2) for the non-magnetic case ((*a*) $J=0$), weak exchange interaction ((*b*) $J/\alpha k_{\mathrm{F}}=0.1$) and strong exchange ((*c*) $J/\alpha k_{\mathrm{F}}=2.5$). The magnetization in (*b*) and (*c*) is assumed to be parallel to the $\hat{\mathbf{y}}$-axis ($\theta=\phi=\pi/2$). (*d*) Fermi contours and spin quantization direction of the bands depicted in (*a*) at equilibrium and (*e*) in response to an applied current parallel to $\hat{\mathbf{x}}$. (*f*, *g*) Same for the bands depicted in (*c*). (Online version in colour.)

value reads

$$\langle\boldsymbol{\sigma}\rangle_{\pm,\mathbf{k}}=\langle\psi_{\pm,\mathbf{k}}|\boldsymbol{\sigma}|\psi_{\pm,\mathbf{k}}\rangle=\frac{1}{k}\begin{pmatrix}\pm k_y\\ \mp k_x\\ 0\end{pmatrix}=\begin{pmatrix}\pm\sin\xi\\ \mp\cos\xi\\ 0\end{pmatrix}. \tag{3.4}$$

As shown in figure 2*a*, the energy dispersion corresponding to equation (3.2) is not anymore a paraboloid of revolution as in the free-electron case, but the quadric surface generated by the rotation of the two branches $\varepsilon_{+,k>0}$, $\varepsilon_{-,k>0}$ around the energy axis intersecting the Γ point. The radius of the two Fermi discs, $k_{\mathrm{F}+}$ and $k_{\mathrm{F}-}$, can be found by imposing that the total electron density of the system is the same as in the free-electron case, i.e. by solving $\varepsilon_{-,k_{\mathrm{F}-}}=\varepsilon_{+,k_{\mathrm{F}+}}=\varepsilon_{\mathrm{F}}$ for $k_{\mathrm{F}\pm}$. This gives, to first order in α,

$$k_{\mathrm{F}\pm}\approx k_{\mathrm{F}}\mp\frac{m_{\mathrm{e}}^{*}\alpha}{\hbar^2}=k_{\mathrm{F}}(1\mp\eta), \tag{3.5}$$

with $\eta=m_{\mathrm{e}}^{*}\alpha/(\hbar^2 k_{\mathrm{F}})$. Although the total spin polarization in each branch averages out, the direction of $\mathbf{k}$ and the spin orientation are related to each other because of the quantization of the electron spin parallel or antiparallel to the SO field. This, together with the fact that $k_{\mathrm{F}+}\neq k_{\mathrm{F}-}$, has important consequences for the out-of-equilibrium transport properties of an SIA system, notably the creation of a net spin polarization by a charge current. The comparison of figure 2*d* and *e* readily shows how an external electric field $\boldsymbol{\mathcal{E}}$ displaces the two Fermi discs by an amount $\delta k_{\pm}=-e\boldsymbol{\mathcal{E}}\tau_{\pm}/\hbar$, resulting in incomplete cancellation of opposite spin-polarization contributions. Note that, since the scattering rate is generally energy- and wavevector-dependent [61], the resistivity relaxation times

$\tau_\pm$ of the two Fermi discs are different. To first order in α, one may assume, for simplicity, that $\tau_\pm = \tau(1 \mp \eta)$ [13], where τ is the relaxation time of the free-electron gas.

It is thus possible to calculate analytically the current contribution from each subband using the Boltzmann equation and the approximations described above. Omitting standard intermediate steps [61], one has

$$\mathbf{j}_\pm = -e \int \mathbf{v}_{\pm,\mathbf{k}} f^1_{\pm,\mathbf{k}} \, \mathrm{d}\mathbf{k} = \frac{1}{4\pi^2} \frac{e^2 \tau_\pm}{\hbar} \int_{\mathcal{S}_{\mathrm{F}\pm}} \frac{\mathbf{v}_{\pm,\mathbf{k}}}{v_{\pm,\mathbf{k}}} \mathbf{v}_{\pm,\mathbf{k}} \cdot \boldsymbol{\mathcal{E}} \, \mathrm{d}\mathcal{S}_\mathrm{F}, \tag{3.6}$$

where $f^1_{\pm,\mathbf{k}} = (\partial f^0/\partial \varepsilon) e \tau_\pm v_{\pm,\mathbf{k}} \cdot \boldsymbol{\mathcal{E}}$ represents the deviation of the electron distribution function from its equilibrium value $f^0_{\pm,\mathbf{k}}$ for the $\pm$ bands and $\mathcal{S}_{\mathrm{F}\pm}$ denotes integration over the respective Fermi surfaces, which in this case are two circles. By choosing $\boldsymbol{\mathcal{E}} = \mathcal{E}\hat{\mathbf{x}}$ and noting that the assumption of electron density equal to the free-electron case implies $v_{\mathrm{F}\pm} = v_\mathrm{F}$, the expression for the current density can be further simplified as

$$j_{\pm,x} = \frac{e^2 \tau_\pm \mathcal{E}}{4\pi^2 \hbar} \int_0^{2\pi} v_\mathrm{F} \cos^2 \xi \, k_{\mathrm{F}\pm} \, \mathrm{d}\xi = \frac{e^2 \mathcal{E}}{4\pi\hbar} v_\mathrm{F} k_{\mathrm{F}\pm} \tau_\pm. \tag{3.7}$$

Thus the total current density is

$$j = j_+ + j_- = \frac{e^2 \mathcal{E}}{2\pi\hbar} v_\mathrm{F} k_\mathrm{F} \tau (1 + \eta^2). \tag{3.8}$$

The partial non-equilibrium spin density can be calculated in an analogous way as

$$\begin{aligned} \langle \delta\boldsymbol{\sigma} \rangle_\pm &= \int \langle \boldsymbol{\sigma} \rangle_{\pm,\mathbf{k}} f^1_{\pm,\mathbf{k}} \, \mathrm{d}\mathbf{k} = \frac{1}{4\pi^2} \frac{-e\tau_\pm}{\hbar} \int_{\mathcal{S}_{\mathrm{F}\pm}} \frac{1}{k} \begin{pmatrix} \pm k_x \\ \mp k_y \\ 0 \end{pmatrix} \frac{\mathbf{v}_{\pm,\mathbf{k}}}{v_{\pm,\mathbf{k}}} \cdot \boldsymbol{\mathcal{E}} \, \mathrm{d}\mathcal{S}_\mathrm{F} \\ &= \frac{-e\tau_\pm \mathcal{E}}{4\pi^2 \hbar} \int_0^{2\pi} \begin{pmatrix} \pm \sin \xi \\ \mp \cos \xi \\ 0 \end{pmatrix} \cos \xi k_{\mathrm{F}\pm} \, \mathrm{d}\xi = \pm \frac{e\mathcal{E}}{4\pi\hbar} \tau_\pm k_{\mathrm{F}\pm} \hat{\mathbf{y}}. \end{aligned} \tag{3.9}$$

Adding the partially compensating contributions from the $\pm$ subbands yields the total non-equilibrium spin density

$$\langle \delta\boldsymbol{\sigma} \rangle = \langle \delta\boldsymbol{\sigma} \rangle_+ + \langle \delta\boldsymbol{\sigma} \rangle_- \approx \frac{-e\mathcal{E}\tau}{\pi\hbar} k_\mathrm{F} \eta \hat{\mathbf{y}} \tag{3.10}$$

approximated to first order in α. By means of equation (3.8), the above expression can be written as

$$\langle \delta\boldsymbol{\sigma} \rangle \approx -\frac{m_\mathrm{e}^* \alpha}{e\hbar\varepsilon_\mathrm{F}} j \hat{\mathbf{y}}. \tag{3.11}$$

This formula exemplifies the action of the effective SO field defined in equation (2.5) on the conduction electrons that move with average wavevector $\langle \mathbf{k} \rangle$ in response to an external electric field. Note that if j is expressed in units of $\mathrm{A\,m^{-1}}$ ($\mathrm{A\,m^{-2}}$), $\langle \delta\boldsymbol{\sigma} \rangle$ has $\mathrm{m^{-2}}$ ($\mathrm{m^{-3}}$) units. The current-induced spin polarization is then $P = 2\langle \delta\sigma \rangle/(\hbar n)$, where n is the charge carrier density.

Although this is a simplified calculation, it turns out that the magnitude of the current-induced spin accumulation is close to that of more complex estimates and independent of the resistivity relaxation time [55], i.e. that equation (3.11) applies to both the 'dirty' and 'clean' conduction limits of fast and slow scattering rate compared with the SO precession rate, respectively [13]. The important qualitative result is that a net spatially uniform spin accumulation can be induced by the flow of an electric current in an SIA or a BIA conductor; the orientation of the non-equilibrium spin density is always transverse to the average electron momentum in the case of Rashba SIA, but depends on the relative alignment between current and crystallographic axes according to the specific form of the SO Hamiltonian in the general case where both SIA and BIA are present.

4. Current-induced spin–orbit torques

(*a*) *Combined effects of exchange and spin–orbit coupling in ferromagnets*

The results of the previous section show that it is possible to manipulate the polarization of the conduction electron spin in the absence of external magnetic fields in either BIA or SIA systems. Together with other forms of spin accumulation and spin currents that can be excited in semiconductors by electrical or optical means, this has generated considerable interest in a 'magnet-free' approach to spintronics [14]. Moreover, several proposals have been made to exploit the intrinsic SO fields in semiconductors to control or modulate spin injection into FM electrodes through a semiconductor channel [62–64] or tunnel junction [31,65,66]. It has been realized as well that the mechanism described in §3 could be used to exert a torque on the magnetization of an FM layer in contact with a semiconducting channel by absorption of the SO-induced spin-polarization component perpendicular to the FM magnetization at the interface between the two materials [67,68]. More recently, however, it has become clear that the very same SO effect is intrinsic also to an FM [69] and can be used to induce a torque on the local magnetization in a single, uniformly magnetized FM structure [15–17] as well as DW motion in FM layers [59]. Here, we focus on such an effect in a uniformly magnetized FM, which we denote as an *SO torque* in order to distinguish it from the widely investigated STT mechanism, where the SO interaction enters only indirectly through the damping and spin-flip relaxation parameters [70].

The combined action of SO coupling and exchange interaction in a single FM layer with either SIA or BIA is described by the Hamiltonian

$$\mathcal{H} = \frac{\hbar^2 k^2}{2m_{\mathrm{e}}^*} + \mathcal{H}_{\mathrm{SO}} - J\hat{\mathbf{M}} \cdot \boldsymbol{\sigma}, \tag{4.1}$$

where $\mathcal{H}_{\mathrm{SO}}$ is defined in equations (2.1)–(2.3), $\hat{\mathbf{M}} = \mathbf{M}/M_{\mathrm{s}}$ is an adimensional unit vector, M_{s} the saturation magnetization of the FM ($\mathrm{A\,m^{-1}}$ units) and J (eV units) the exchange coupling parameter between the conduction electron spin and the local moments of the FM. The physical picture described by equation (4.1) is that, even though the spin of the conduction electrons in an FM is usually aligned parallel or antiparallel to the local magnetization $\mathbf{M}$, an out-of-equilibrium spin

density non-collinear to **M** is created by the flow of a current. This component interacts with **M** through the exchange coupling between itinerant and localized electrons, i.e. between p–d and s–d states in a magnetic semiconductor and transition metal, respectively, in a way analogous to a magnetic field with fixed orientation, determined by the current and crystal structure.

In the case of the pure Rashba interaction, diagonalization of equation (4.1) for an arbitrary direction of $\hat{\mathbf{M}} = (\sin\theta\cos\phi, \sin\theta\sin\phi, \cos\theta)$ and electric current $\mathbf{j} = j(\cos\xi, \sin\xi, 0)$ confined to the azimuthal plane yields the energy eigenvalues

$$\varepsilon_{\pm,\mathbf{k}} = \frac{\hbar^2 k^2}{2m_e^*} \pm \sqrt{J^2 + \alpha^2 k^2 - 2\alpha k J \sin\theta \sin(\xi - \phi)}. \tag{4.2}$$

The resulting band structure thus depends on the relative strength of exchange versus SO-induced spin splitting, i.e. on the ratio $J/\alpha k_F$, as shown in figure 2*a–c*. Note that gradually turning on exchange results first in the opening of a gap of magnitude $2J$ between $\varepsilon_{+,\mathbf{k}}$ and $\varepsilon_{-,\mathbf{k}}$ at $k = 0$ and, finally, to fully spin-polarized spin-up and spin-down bands where the Rashba interaction acts only as a perturbation. The band asymmetry in figure 2*b*,*c* depends on the relative orientation of **k** with respect to **M**, and disappears for $\mathbf{M} \parallel \hat{\mathbf{z}}$.

Manchon & Zhang [15] carried out the explicit calculation of the non-equilibrium spin density $\langle\delta\boldsymbol{\sigma}\rangle$ induced by the flow of an electric current in an FM in a way analogous to the procedure described in §3 with the addition of exchange. However, the order of magnitude of the effective field acting on **M** can be estimated in an even simpler way. Supposing that exchange coupling is weak relative to the SO interaction, then $\langle\delta\boldsymbol{\sigma}\rangle$ can be calculated to first order in α and zeroth order in J, giving the same result as equation (3.11). By writing the cost in exchange energy per unit volume owing to $\langle\delta\boldsymbol{\sigma}\rangle$ (m^{-3} units) as $-J\langle\delta\boldsymbol{\sigma}\rangle \cdot \hat{\mathbf{M}}$, one can easily see that the action of a current on the local moments is equivalent to that of an induction magnetic field (T units)

$$\mathbf{B}_{\mathrm{SO}} = J\frac{\langle\delta\boldsymbol{\sigma}\rangle}{M_s} = -\frac{m_e^*\alpha}{e\hbar M_s} Pj\,(\hat{\mathbf{z}} \times \hat{\mathbf{j}}), \tag{4.3}$$

or to that of a torque per unit volume

$$\mathbf{T}_{\mathrm{SO}} = \hat{\mathbf{M}} \times J\langle\delta\boldsymbol{\sigma}\rangle = \frac{m_e^*\alpha}{e\hbar} Pj(\hat{\mathbf{M}} \times \hat{\mathbf{y}}), \tag{4.4}$$

where the parameter $P = J/\varepsilon_F$ is approximately equal to the spin polarization of the current. It can be shown that a thorough calculation of $\langle\delta\boldsymbol{\sigma}\rangle$ in the case of strong exchange coupling ($J \gg \alpha k_F$) yields the same result of equations (4.3) and (4.4) [15,16].[1]

A similar calculation can be performed in the general case of coexisting Rashba and Dresselhaus SO interactions [17]. The effective fields corresponding to $\mathcal{H}_{\mathrm{SO}}$ of equations (2.1)–(2.3) are

$$\mathbf{B}_{\mathrm{SO}_{(100)}} = \frac{m_e^*\alpha}{e\hbar M_s} Pj[(-\alpha\sin\xi - \gamma\cos\xi)\hat{\mathbf{x}} + (\alpha\cos\xi - \gamma\sin\xi)\hat{\mathbf{y}}], \tag{4.5}$$

[1]Note that eqns (7), (11) and (12) in Manchon & Zhang [15] report an erroneous factor 2.

$$\mathbf{B}_{\mathrm{SO}_{(110)}} = \frac{m_{\mathrm{e}}^{*}\alpha}{e\hbar M_{\mathrm{s}}} Pj[-\alpha \sin\xi\hat{\mathbf{x}} - \cos\xi(\beta\hat{\mathbf{y}} + \lambda\hat{\mathbf{z}})] \tag{4.6}$$

and

$$\mathbf{B}_{\mathrm{SO}_{(111)}} = \frac{m_{\mathrm{e}}^{*}\alpha}{e\hbar M_{\mathrm{s}}} Pj(-\alpha + \gamma)(\sin\xi\hat{\mathbf{x}} - \cos\xi\hat{\mathbf{y}}). \tag{4.7}$$

An alternative way to look at this phenomenon has been introduced by Garate & MacDonald [71] by calculating the change in magnetocrystalline anisotropy energy induced by the flow of a steady-state electric current in a non-centrosymmetric FM conductor. This follows from the general definition of the internal anisotropy field of an FM as the derivative of the ground-state energy with respect to the direction of the magnetization, analogously to the derivation of the effective magnetic field that enters into the Landau–Lifshitz equation of magnetization dynamics. As the electric current breaks time reversal invariance, the magnetic anisotropy energy in the transport steady state of an FM turns out to be unidirectional, i.e. not invariant with respect to magnetization reversal. It can be shown that the contribution to the anisotropy field owing to the applied current is directly related to the non-equilibrium transverse spin density $\langle\delta\boldsymbol{\sigma}\rangle$ calculated above.

(*b*) *Spin–orbit versus spin torque*

It is of interest to analyse the distinctive features of the SO torque or, equivalently, of the effective field $\mathbf{B}_{\mathrm{SO}}$ with respect to other known types of current-induced torques in magnetic materials. The general form of the modified Landau–Lifshitz–Gilbert equation that takes into account STT terms [70,72] together with the SO interaction in a single magnetic layer characterized by inversion asymmetry can be written as

$$\frac{\partial\mathbf{M}}{\partial t} = \gamma_{\mathrm{e}}\mathbf{M}\times(\mathbf{B}_{\mathrm{ext}} + \mathbf{B}_{\mathrm{exc}} + \mathbf{B}_{\mathrm{an}} + \mathbf{B}_{\mathrm{SO}}) + \frac{\lambda_G}{M_{\mathrm{s}}}\mathbf{M}\times\frac{\partial\mathbf{M}}{\partial t} - \frac{1}{(1+\beta^2)M_{\mathrm{s}}^2}\mathbf{M}\times[\mathbf{M}\times(\mathbf{u}\cdot\nabla)\mathbf{M}] - \frac{\beta}{(1+\beta^2)M_{\mathrm{s}}}\mathbf{M}\times(\mathbf{u}\cdot\nabla)\mathbf{M}, \tag{4.8}$$

where $\gamma_{\mathrm{e}} = -e/m_{\mathrm{e}}$ is the gyromagnetic ratio, $\mathbf{B}_{\mathrm{ext}}$, $\mathbf{B}_{\mathrm{exc}}$ and $\mathbf{B}_{\mathrm{an}}$ represent the external, exchange and anisotropy magnetic fields, λ_{G} is the Gilbert damping parameter and $\beta = \hbar/(J\tau_{\mathrm{sf}})$ is the non-adiabaticity parameter, which depends on the s–d exchange and the spin-flip relaxation time τ_{sf}. The vector $\mathbf{u} = (\mu_{\mathrm{B}}P/eM_{\mathrm{s}})\mathbf{j}$ represents the action of a spin-polarized current on the magnetization gradient, yielding the adiabatic and non-adiabatic STT contributions, i.e. the last two terms of equation (4.8).

The adiabatic and non-adiabatic STT components can be observed by injecting a current into a textured magnetic film, i.e. in measurements of DW displacements [73–75]. Although these two torques exist independently of SIA or BIA, a recent experiment revealed an enhancement of the non-adiabatic spin torque component in an SIA Co film deposited between asymmetric Pt and Al oxide interfaces [76]. Such an enhancement can be related to the increase in the conduction electron spin-flip rate $1/\tau_{\mathrm{sf}}$ caused by the SO interaction. The difference between this effect and a proper SO torque can be understood by considering the single- and many-electron pictures. In the single-electron case, the

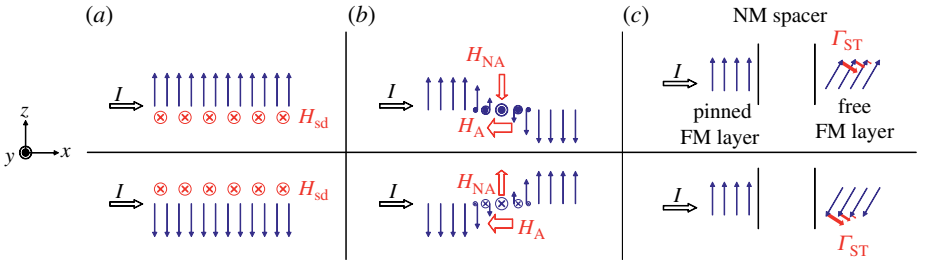

Figure 3. Cross-sectional schematic of the different types of effective magnetic fields generated by (*a*) Rashba torque, (*b*) adiabatic and non-adiabatic spin torque, and (*c*) spin-transfer torque. The bottom panels show the field/torque directions (thick arrows) under reversal of the magnetization (thin arrows). (Online version in colour.)

field given by the SO interaction induces the rotation of the spin around an axis perpendicular to the electric field and the instantaneous wavevector **k**. In a many-electron picture, however, the rotation of the spins has a collective component, owing to $\mathbf{B}_{SO}$, as well as a dispersive component, owing to the distribution of **k** on the Fermi sphere. This second component leads to spin decoherence, i.e. a decrease in τ_{sf}. Equation (4.8) shows that the non-adiabatic STT term may be enhanced by the latter effect, conditional on the presence of a magnetization gradient. As shown in figure 3, the field-equivalent of the non-adiabatic STT component has different symmetry and time-reversal properties compared with $\mathbf{B}_{SO}$. Thus, despite their common origin, these two mechanisms are qualitatively and quantitatively different, producing distinct effects on the local magnetization.

Generally speaking, the main differences between STT and SO torques, sketched in figure 3 for the specific case of Rashba SO coupling, can be summarized as follows. First, whereas STT works by transferring *spin* angular momentum between two non-collinear magnetic layers or domains, an SO torque transfers *orbital* momentum from the lattice to the spin system. It is therefore independent of the magnetic configuration of the layer and homogeneously distributed inside a magnetic film, whereas STT requires the presence of a magnetization gradient $(\mathbf{u}\cdot\nabla)\mathbf{M}\neq 0$. From equations (4.5) to (4.8), it follows that the action of $\mathbf{B}_{SO}$ is analogous to that of an externally applied field, the sign of which depends on the current direction but is independent of the local magnetization orientation. As such, $\mathbf{B}_{SO}$ can be used to switch the magnetization of a single FM layer by current injection without the need of a fixed magnetic 'polarizer' and non-magnetic spacer layers, as required by STT devices. However, $\mathbf{B}_{SO}$ is an effective field with orientation defined by the current direction with respect to the crystalline structure of the FM; therefore, it cannot be used to excite steady magnetization precession, contrary to the negative damping term introduced by STT [77,78].

(*c*) *Spin–orbit torque in dilute magnetic semiconductors*

The experimental detection of a Dresselhaus type of SO torque in an FM was first reported by Chernyshov *et al.* [18] for dilute magnetic semiconductor $Ga_{1-x}Mn_xAs$ films epitaxially grown on the (001) surface of GaAs. The films, with Mn concentration $x = 6$–7%, present FM behaviour up to a Curie temperature

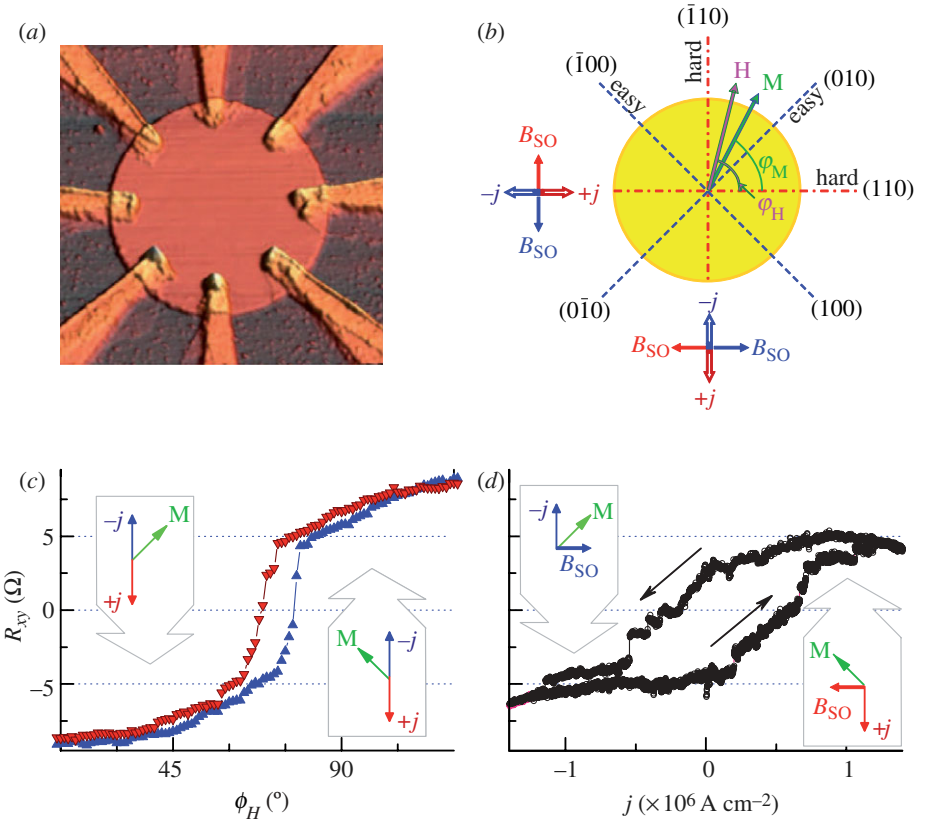

Figure 4. (*a*) Atomic force micrograph of a 6 µm wide $Ga_{1-x}Mn_xAs$ disc with non-magnetic contacts aligned along the crystallographic directions shown in (*b*). (*c*) Transverse anisotropic magnetoresistance R_{xy} as a function of external field direction ϕ_H for $H = 10$ mT and $j = \pm 1 \times 10^6$ A cm^{-2}. (*d*) Current-driven variation of R_{xy} for a fixed field $H = 6$ mT applied at $\phi_H = 72°$, showing the hysteretic rotation of **M** from the [010] to the [1̄00] direction. Adapted from Chernyshov *et al.* [18] with permission from the authors. (Online version in colour.)

of about 80 K. Compressive strain in this system leads to in-plane fourfold magnetic anisotropy with two easy axes along the [100] and [010] directions and an SO field of the linear Dresselhaus type given by equations (2.1) with $\alpha = 0$, and $\gamma \approx 2 \times 10^{-13}$ eV m, proportional to the difference between out-of-plane and in-plane diagonal components of the strain tensor. The action of the effective SO magnetic field was detected in 10–15 nm thick films patterned into discs of diameter up to 10 µm by measuring the transverse anisotropic magnetoresistance, $R_{xy} = V_y/I_x$ (figure 4*a*), as a function of the direction and magnitude of the injected current and externally applied magnetic field **H**: $R_{xy} \propto (\rho_\parallel - \rho_\perp) \cos\phi_M \sin\phi_M$, where $\rho_\parallel$ ($\rho_\perp$) denote the resistivity for $\mathbf{j} \parallel \mathbf{M}$ ($\mathbf{j} \perp \mathbf{M}$) and the angle ϕ_M is defined in figure 4*b*. By mapping the angular dependence of $\mathbf{B}_{SO}$ for both $\mathbf{j} \parallel [1\bar{1}0]$ and $\mathbf{j} \parallel [110]$, Chernyshov *et al.* showed that $\mathbf{B}_{SO}$ presents the symmetry expected from equation (4.5) in the absence of a Rashba component, i.e. that of figure 1*b*. Figure 4*c* reports the change in sign of R_{xy} owing to the

rotation of ϕ_M by 90° as **M** switches from the easy direction parallel to [010] to the easy direction parallel to [$\bar{1}$00] under an in-plane applied field of constant amplitude and variable direction ϕ_H. Hysteretic behaviour is observed as the current direction is reversed, because switching occurs at a lower angle ϕ_H when both the projections of $\mathbf{B}_{\mathrm{SO}}$ and **H** along one of the easy axes have a positive sign. Reversible field-assisted magnetization switching controlled by the current direction could thus be demonstrated in the presence of a fixed external field of 6 mT applied at $\phi_H = 72°$ for a current density $|j| \gtrsim 10^6\,\mathrm{A\,cm^{-2}}$, as shown in figure 4*d*. The critical current required to induce switching is about a factor 10 larger compared with the STT mechanism in $Ga_{1-x}Mn_xAs$ [79], but still compares favourably with respect to metal-based STT devices [3]. Notably, the saturation magnetization M_s enters equations (4.4)–(4.6) through a denominator, which favours low switching thresholds in dilute magnetic semiconductors owing to their relatively small M_s compared with FM metals. Because the symmetry of $\mathbf{B}_{\mathrm{SO}}$ can be adjusted through epitaxial strain and stacking of different layers, and both M_s and J can be controlled through the charge carrier density, dilute magnetic semiconductors represent very rich systems for future investigations of SO torques and related effects.

(*d*) *Spin–orbit torques in ultrathin metal films*

Experimental studies of current-induced SO effects have traditionally focused on semiconductors since bulk metals present centrosymmetric crystal structures. However, Rashba-type SO splitting of the conduction bands can still take place at the interface between a metal and a dissimilar material, including vacuum. This was first recognized in angle-resolved photoemission measurements of the surface states of non-magnetic 5d elements, in particular Au [32,80,81], W [82] and Bi [83]. Investigations of rare-earth surface states, notably of Gd [34] and Tb [42], later revealed clear signatures of coexisting Rashba and exchange coupling in the case of FM metal films in the form of magnetization-dependent asymmetry of the electron band dispersion, similar to that sketched in figure 2*c*. These studies coincide in showing that a heavy metal interface induces large Rashba splittings of the order of 100 meV and that increasing the asymmetry of the charge distribution at a metal surface leads to an increase of such an effect [34,84,85], in agreement with equation (2.6).

The necessary conditions to induce an SO torque are therefore fulfilled in metal systems as well as in semiconductors. Recently, Miron *et al.* [19] reported the first observation of a current-induced SO torque in an FM metal for a thin Co layer grown between asymmetric Pt and AlO_x interfaces. The structure of this system, shown in figure 5*a*, was chosen so as to optimize the SIA of the FM Co layer and produce a strong Rashba effect. Experiments were performed on a 0.6 nm thick Co film sandwiched between 3 nm Pt and 1.6 nm Al layers deposited by sputtering on a thermally oxidized Si wafer. The top Al layer was exposed to an oxygen radio-frequency plasma resulting in a fully oxidized AlO_x interface at the Co boundary [86,87]. SIA results from the presence of AlO_x and Pt on either side of the Co layer, where Pt/Co hybridization enhances atomic SO coupling and both interfaces create a strong out-of-plane electron potential gradient. Measurements of the magnetic anisotropy energy and orbital magnetization of Co/Pt [88–90], the AHE as well as the enhanced non-adiabatic spin torque component found in

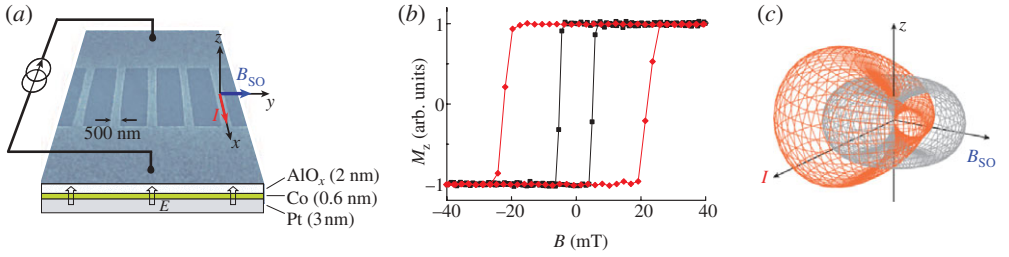

Figure 5. (*a*) Scanning electron micrograph detail of the patterned Pt/Co/AlO_x wire array and schematic vertical cross section of the layer. Arrows indicates the direction of the current (**j**), interfacial electric field (**E** ∥ $\hat{\mathbf{z}}$) and $\mathbf{B}_{SO}$. The sign of **E** is determined from the measured orientation of **j** and $\mathbf{B}_{SO}$ assuming positive polarization of the conduction electrons near the Fermi level. (*b*) Perpendicular magnetization of Pt/Co/AlO_x (diamonds) and Pt/Co/Pt (squares) measured at room temperature by AHE. (*c*) Three-dimensional energy surface of a uniaxial monodomain FM system with SIA in the absence (presence) of current. (Online version in colour.)

Pt/Co/AlO_x DW constrictions [76] indicate that SO coupling in such a system is strong. Most importantly, the Co layer is FM at room temperature with 100 per cent remanence, as shown in figure 5*b*. The Co magnetization has a saturation value close to the bulk, $M_s = 1090\,\mathrm{kA\,m^{-1}}$, and is very stable after oxidation. For control purposes, a symmetric structure Pt/Co/Pt was grown by replacing the AlO_x layer with 3 nm Pt, giving a saturation magnetization of $1110\,\mathrm{kA\,m^{-1}}$. Both samples present strong out-of-plane anisotropy and uniaxial anisotropy fields of 0.92 and 0.57 T, determined as the field required to achieve 90 per cent magnetic polarization along the hard axis.

In order to observe the effects of current injection on **M**, the two films were patterned into an array of wires, each 0.5 µm wide and 5 µm long, and contacted by two current pads. In this geometry, the application of a current is expected to produce an in-plane field $\mathbf{B}_{SO}$ perpendicular to the wires, as given by equation (4.3). By itself, this field will not induce deterministic switching of **M** between the up and down directions. However, if $\mathbf{B}_{SO}$ is sufficiently strong compared with the anisotropy field, the energy barrier for magnetization reversal will be distorted from the symmetric doughnut shape typical of uniaxial anisotropy to a strongly asymmetric profile, lowering the barrier in the $\hat{\mathbf{j}} \times \hat{\mathbf{z}}$ direction and raising it in the opposite one, as shown in figure 5*c*. Such a current-induced distortion can be compensated or enhanced by applying an in-plane external field B_{ext} collinear to it, providing a means to quantify the magnitude of B_{SO}. Starting from a monodomain out-of-plane configuration, the Co magnetization was monitored using wide-field polar Kerr microscopy as single current pulses of increasing amplitude and constant 100 ns duration were injected into the wires until the nucleation of reversed domains was observed. This occurred as the wires evolved from the saturated metastable monodomain state towards the macroscopically demagnetized ground state constituted by an equal mixture of up and down domains. Figure 6*a* shows that about an equal amount of nucleation events occurs at a current density $j = 7.8 \times 10^7\,\mathrm{A\,cm^{-2}}$ for opposite current directions if $B_{ext} = 0$. However, as $B_{ext} \lessgtr 0$, the domain nucleation rate

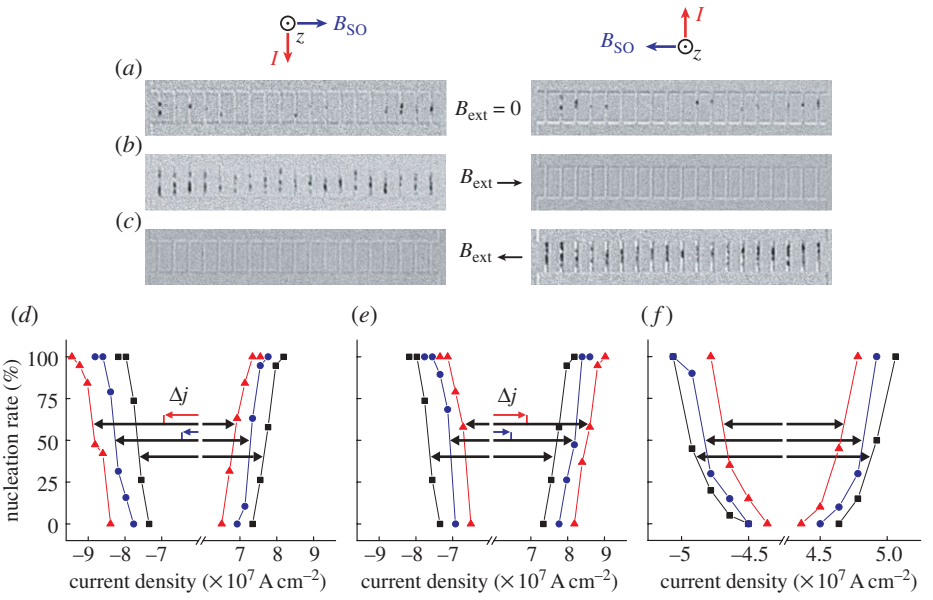

Figure 6. Difference between consecutive Kerr microscopy images of Pt/Co/AlO_x wires recorded before and after current pulse injection for (*a*) $B_{ext} = 0$, (*b*) $B_{ext} = +47.5$ mT, (*c*) $B_{ext} = -47.5$ mT and positive (left) and negative (right) current values at constant pulse amplitude $j = 7.8 \times 10^7$ A cm^{-2}. (*d–f*) Percentage of wires that present reversed magnetic domains after the injection of a current pulse as a function of j and B_{ext}. (*a*) Pt/Co/AlO_x, $\mathbf{B}_{ext} \parallel \hat{\mathbf{y}}$; (*b*) Pt/Co/$AlO_x$, $\mathbf{B}_{ext} \parallel -\hat{\mathbf{y}}$; (*c*) Pt/Co/Pt, $\mathbf{B}_{ext} \parallel -\hat{\mathbf{y}}$. Values of B_{ext} are 0 mT (squares), ±47.5 mT (dots), ±95 mT (triangles). (Online version in colour.)

becomes strongly asymmetric depending on the relative orientation of current and field (figure 6*b*,*c*). These results qualitatively prove the presence of a current-induced torque acting on the Co magnetization with the symmetry properties predicted by equation (4.3). It should be noted that Joule heating caused by the current may also lower the domain nucleation barrier, but cannot explain the asymmetry of the nucleation rate observed at constant j. Artefacts owing to a small unintentional misalignment of B_{ext} outside the xy-plane are also ruled out, as these would be independent of the sign of j. Further, the Oersted field acting on Co produced by the current flowing in the Pt layer would have opposite effects compared with those observed in figure 6, and an estimated magnitude of less than 1 mT $\ll B_{ext}$. Finally, similar measurements performed on Pt/Co/Pt do not yield any measurable asymmetry in the nucleation rate, providing a final proof of the SO origin of the torque in Pt/Co/AlO_x related to SIA.

The quantitative dependence of B_{SO} on j was determined by making systematic use of B_{ext} as a known reference field, and plotting the percentage of wires for which at least one nucleation event was observed for a given combination of B_{ext} and j, as reported in figure 6*d–f*. Strong amplification or suppression of domain nucleation was observed depending on the orientation and amplitude of the current density and external field, leading to a rigid shift Δj of the nucleation rate curves measured for different values of B_{ext}. The inverse slope of the (B_{ext}, Δj) plot, reported in figure 7 for both Pt/Co/AlO_x and Pt/Co/Pt, is a direct

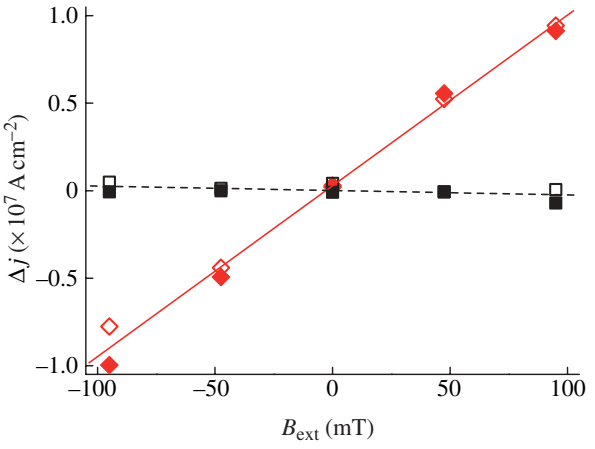

Figure 7. Variation of the current amplitude required to observe domain nucleation in 50% of the wires as a function of B_{ext}. Diamonds correspond to $Pt/Co/AlO_x$, squares to Pt/Co/Pt. Filled and open symbols refer to samples initially magnetized up ($\parallel \hat{\mathbf{z}}$) and down ($\parallel -\hat{\mathbf{z}}$), respectively. The lines are linear fits to the data. Filled diamonds, $Pt/Co/AlO_x$, M_0 up; open diamonds, $Pt/Co/AlO_x$, M_0 down; filled squares, Pt/Co/Pt, M_0 up; open squares, Pt/Co/Pt, M_0 down. (Online version in colour.)

measure of the B_{SO}/j ratio, giving $(1.0 \pm 0.1) \times 10^{-8}\,\mathrm{T\,cm^2\,A^{-1}}$. This value shows that the SO torque acting on the Co magnetization is extremely large, matching the prediction of equation (4.3) for a Rashba constant $\alpha = 10^{-10}\,\mathrm{eV\,m}$, which is a realistic estimate considering that α ranges from 4×10^{-11} to $3 \times 10^{-10}\,\mathrm{eV\,m}$ at the interface of 5d metal systems and that oxidation may further enhance its value. We remark, however, that recent AHE measurements show that the relationship between B_{SO} and j is not linear, in particular when an extended range of currents $j = 10^6 - 10^8\,\mathrm{A\,cm^{-2}}$ is considered [91,92]. Such nonlinear behaviour might be attributed to transient heating effects, which, at high current, can enhance the effective action of B_{SO} compared with static external fields, as well as to more complex dynamic phenomena that are not included in the simple models presented here [92].

The structural origin of the SO-induced magnetic fields is different in $Pt/Co/AlO_x$ compared with the case of $Ga_{1-x}Mn_xAs$ discussed in the previous section, the first being due to the Rashba effect and the second to the Dresselhaus effect. Note that, according to equations (4.5)–(4.7), the lower M_{s} favours a greater efficacy of the SO field in $Ga_{1-x}Mn_xAs$ relative to $Pt/Co/AlO_x$; the much larger value of α in $Pt/Co/AlO_x$ compared with γ in $Ga_{1-x}Mn_xAs$, however, compensates for this effect. Moreover, as the current flows in both Co and Pt layers, the measured B_{SO}/j ratio in $Pt/Co/AlO_x$ depends also on the SO torque acting on the Pt-induced magnetization [88]. There are reasons to believe that the SO torque efficacy may be further enhanced in FM metals through proper interface engineering and/or alloying with high Z atoms. Photoemission studies revealed the presence of giant SO splitting at Ag and Si (111) surfaces alloyed with Bi [39,93] as well as the possibility to tune the spin-dependent density of states near ε_{F} by quantum well effects [94–97].

We note here that the realization of the role played by the Rashba effect in FM metals may help the interpretation of past experimental puzzles and suggest future directions for fundamental as well as applied research. For instance, the extraordinarily high transient magnetic anisotropy attributed to the electric field produced by a relativistic electron bunch traversing a $Cr_{80}Mg_{20}/Co_{70}Fe_{30}/Pt$ layer [98] could be interpreted as the action of a transient SO field owing to the equivalent current density of the bunch. At the fundamental level, the relationship between α and magnetocrystalline anisotropy energy should be further studied, as both depend on the strength of the SO interaction and it is not yet clear how the presence of strong electric gradients across dissimilar interfaces relates quantitatively to the occurrence of perpendicular magnetic anisotropy.

5. Outlook

The experimental discovery of a Rashba-type torque in an FM metal at room temperature [19] opens very promising perspectives in spintronics, namely for the fabrication of magnetic storage and logic gates operating through intrinsic current-induced SO torques. By controlling the magnetization orientation through the interplay of magnetocrystalline and shape anisotropy, materials and geometries appropriate for switching without the assistance of external magnetic fields can be realized. The single FM layer structure, robust FM properties of metal films, and the possibility of modulating the Rashba field by an external gate voltage [36] allow for the design of novel and simplified devices with respect to those currently investigated in mainstream spintronics. However, SO torques may also be readily integrated in existing technological platforms. Indeed, a metal/oxide bilayer is already half of an MTJ, which could be used as a readout element of a magnetic bit where the write functions are performed by the SO torque [15]. Moreover, several studies have pointed out the interplay between SO coupling and tunnelling anisotropic magnetoresistance in MTJs [99–101] and explicitly considered the dependence of the tunnelling conductance on interfacial Rashba spin splitting in metal systems [102,103] as well as the coexistence of Dresselhaus and Rashba fields in metal/semiconductor heterojunctions [31,65,104], providing additional functionalities to layers displaying strong SO effects. Further, as noted by Obata & Tatara [59], DW manipulation can be achieved by means of an SO torque, depending on the type of DW involved and easy axis magnetization direction, which may be useful in, for example, shift register or random access memory applications based on DW motion.

In conclusion, theoretical predictions and experimental observations show that strong SO torques acting on uniformly magnetized FM layers can be induced by the flow of an electric current. SO torques originate from either SIA or BIA in combination with sp–d exchange, allowing for the transfer of orbital angular momentum from the crystal lattice to the local spin magnetization. Because of the intrinsic coupling between charge and spin, SO torques are equivalent to an effective magnetic field and can be induced in uniformly magnetized layers without the need of non-collinear polarization layers, contrary to STT. The current densities required to produce sizeable SO-induced fields are in the range $10^6-10^8\,\mathrm{A\,cm^{-2}}$, comparable to those required by STT device operation.

We thank A. Mugarza and H. Szambolics for useful discussions and L. P. Rokhinson for the permission to reproduce the data reported in figure 4. The work was supported by the European Research Council (StG 203239-NOMAD), the Spanish Ministerio de Ciencia e Innovación (ERA-Net EUI2008-03884, MAT2010-15659), and Catalan Agència de Gestió d'Ajuts Universitaris i de Recerca (2009 SGR 695).

References

1 Slonczewski, J. C. 1996 Current-driven excitation of magnetic multilayers. *J. Magn. Magn. Mater.* **159**, L1–L7. (doi:10.1016/0304-8853(96)00062-5)
2 Berger, L. 1996 Emission of spin waves by a magnetic multilayer traversed by a current. *Phys. Rev. B* **54**, 9353–9358. (doi:10.1103/PhysRevB.54.9353)
3 Ralph, D. & Stiles, M. 2008 Spin transfer torques. *J. Magn. Magn. Mater.* **320**, 1190–1216. (doi:10.1016/j.jmmm.2007.12.019)
4 Ohno, H., Chiba, D., Matsukura, F., Omiya, T., Abe, E., Dietl, T., Ohno, Y. & Ohtani, K. 2000 Electric-field control of ferromagnetism. *Nature* **408**, 944–946. (doi:10.1038/35050040)
5 Laukhin, V. *et al.* 2006 Electric-field control of exchange bias in multiferroic epitaxial heterostructures. *Phys. Rev. Lett.* **97**, 227201. (doi:10.1103/PhysRevLett.97.227201)
6 Chu, Y.-H. *et al.* 2008 Electric-field control of local ferromagnetism using a magnetoelectric multiferroic. *Nat. Mater.* **7**, 478–482. (doi:10.1038/nmat2184)
7 Weisheit, M., Fahler, S., Marty, A., Souche, Y., Poinsignon, C. & Givord, D. 2007 Electric field-induced modification of magnetism in thin-film ferromagnets. *Science* **315**, 349–351. (doi:10.1126/science.1136629)
8 Maruyama, T. *et al.* 2009 Large voltage-induced magnetic anisotropy change in a few atomic layers of iron. *Nat. Nanotechnol.* **4**, 158–161. (doi:10.1038/NNANO.2008.406)
9 Dyakonov, M. & Perel, V. 1971 Possibility of orienting electron spins with current. *JETP Lett.* **13**, 467–469.
10 Ivchenko, E. & Pikus, G. 1978 New photogalvanic effect in gyrotropic crystals. *JETP Lett.* **27**, 604–608.
11 Aronov, A. G. & Lyanda-Geller, Y. B. 1989 Nuclear electric resonance and orientation of carrier spins by an electric field. *JETP Lett.* **50**, 431–434.
12 Ganichev, S. & Prettl, W. 2003 Spin photocurrents in quantum wells. *J. Phys. Condens. Matter* **15**, R935–R983. (doi:10.1088/0953-8984/15/20/204)
13 Silsbee, R. 2004 Spin–orbit induced coupling of charge current and spin polarization. *J. Phys. Condens. Matter* **16**, R179–R207. (doi:10.1088/0953-8984/16/7/R02)
14 Awschalom, D. & Samarth, N. 2009 Spintronics without magnetism. *Physics* **2**, 50. (doi:10.1103/Physics.2.50)
15 Manchon, A. & Zhang, S. 2008 Theory of nonequilibrium intrinsic spin torque in a single nanomagnet. *Phys. Rev. B* **78**, 212405. (doi:10.1103/PhysRevB.78.212405)
16 Manchon, A. & Zhang, S. 2009 Theory of spin torque due to spin–orbit coupling. *Phys. Rev. B* **79**, 094422. (doi:10.1103/PhysRevB.79.094422)
17 Matos-Abiague, A. & Rodriguez-Suarez, R. L. 2009 Spin–orbit coupling mediated spin torque in a single ferromagnetic layer. *Phys. Rev. B* **80**, 094424. (doi:10.1103/PhysRevB.80.094424)
18 Chernyshov, A., Overby, M., Liu, X., Furdyna, J. K., Lyanda-Geller, Y. & Rokhinson, L. P. 2009 Evidence for reversible control of magnetization in a ferromagnetic material by means of spin–orbit magnetic field. *Nat. Phys.* **5**, 656–659. (doi:10.1038/NPHYS1362)
19 Miron, I. M., Gaudin, G., Auffret, S., Rodmacq, B., Schuhl, A., Pizzini, S., Vogel, J. & Gambardella, P. 2010 Current-driven spin torque induced by the Rashba effect in a ferromagnetic metal layer. *Nat. Mater.* **9**, 230–234. (doi:10.1038/NMAT2613)
20 Chappert, C., Fert, A. & Van Dau, F. N. 2007 The emergence of spin electronics in data storage. *Nat. Mater.* **6**, 813–823. (doi:10.1038/nmat2024)
21 Winkler, R. 2003 *Spin–orbit coupling effects in two-dimensional electron and hole systems.* Berlin, Germany: Springer.

22 Dresselhaus, G. 1955 Spin–orbit coupling effects in zinc blende structures. *Phys. Rev.* **100**, 580–586. (doi:10.1103/PhysRev.100.580)
23 Bir, G. L. & Pikus, G. E. 1974 *Symmetry and strain-induced effects in semiconductors*. New York, NY: Wiley.
24 Rashba, E. 1960 Properties of semiconductors with an extremum loop. I. Cyclotron and combinational resonance in a magnetic field perpendicular to the plane of the loop. *Sov. Phys. Solid State* **2**, 1109–1122.
25 Casella, R. C. 1960 Toroidal energy surfaces in crystals with wurtzite symmetry. *Phys. Rev. Lett.* **5**, 371–373. (doi:10.1103/PhysRevLett.5.371)
26 Vas'ko, F. T. 1979 Spin splitting in the spectrum of two-dimensional electrons due to surface potential. *JETP Lett.* **30**, 541–544.
27 Bychkov, Y. & Rashba, E. 1984 Oscillatory effects and the magnetic susceptibility of carriers in inversion layers. *J. Phys. C* **17**, 6039–6045. (doi:10.1088/0022-3719/17/33/015)
28 Cartoixà, X., Wang, L. W., Ting, D. Z. Y. & Chang, Y. C. 2006 Higher-order contributions to Rashba and Dresselhaus effects. *Phys. Rev. B* **73**, 205341. (doi:10.1103/PhysRevB.73.205341)
29 Ganichev, S. D. *et al.* 2004 Experimental separation of Rashba and Dresselhaus spin splittings in semiconductor quantum wells. *Phys. Rev. Lett.* **92**, 256601. (doi:10.1103/PhysRevLett.92.256601)
30 Meier, L., Salis, G., Shorubalko, I., Gini, E., Schön, S. & Ensslin, K. 2007 Measurement of Rashba and Dresselhaus spin–orbit magnetic fields. *Nat. Phys.* **3**, 650–654. (doi:10.1038/nphys675)
31 Moser, J., Matos-Abiague, A., Schuh, D., Wegscheider, W., Fabian, J. & Weiss, D. 2007 Tunneling anisotropic magnetoresistance and spin-orbit coupling in Fe/GaAs/Au tunnel junctions. *Phys. Rev. Lett.* **99**, 056601. (doi:10.1103/PhysRevLett.99.056601)
32 LaShell, S., McDougall, B. A. & Jensen, E. 1996 Spin splitting of an Au(111) surface state band observed with angle resolved photoelectron spectroscopy. *Phys. Rev. Lett.* **77**, 3419–3422. (doi:10.1103/PhysRevLett.77.3419)
33 Reinert, F., Nicolay, G., Schmidt, S., Ehm, D. & Hüfner, S. 2001 Direct measurements of the *L*-gap surface states on the (111) face of noble metals by photoelectron spectroscopy. *Phys. Rev. B* **63**, 115415. (doi:10.1103/PhysRevB.63.115415)
34 Krupin, O., Bihlmayer, G., Starke, K., Gorovikov, S., Prieto, J., Dobrich, K., Blugel, S. & Kaindl, G. 2005 Rashba effect at magnetic metal surfaces. *Phys. Rev. B* **71**, 201403. (doi:10.1103/PhysRevB.71.201403)
35 Stormer, H. L., Schlesinger, Z., Chang, A., Tsui, D. C., Gossard, A. C. & Wiegmann, W. 1983 Energy structure and quantized Hall effect of two-dimensional holes. *Phys. Rev. Lett.* **51**, 126–129. (doi:10.1103/PhysRevLett.51.126)
36 Nitta, J., Akazaki, T., Takayanagi, H. & Enoki, T. 1997 Gate control of spin–orbit interaction in an inverted $In_{0.53}Ga_{0.47}As/In_{0.52}Al_{0.48}As$ heterostructure. *Phys. Rev. Lett.* **78**, 1335–1338. (doi:10.1103/PhysRevLett.78.1335)
37 Cercellier, H., Fagot-Revurat, Y., Kierren, B., Reinert, F., Popović, D. & Malterre, D. 2004 Spin–orbit splitting of the Shockley state in the Ag/Au(111) interface. *Phys. Rev. B* **70**, 193412. (doi:10.1103/PhysRevB.70.193412)
38 Popović, D., Reinert, F., Hüfner, S., Grigoryan, V. G., Springborg, M., Cercellier, H., Fagot-Revurat, Y., Kierren, B. & Malterre, D. 2005 High-resolution photoemission on Ag/Au (111): spin–orbit splitting and electronic localization of the surface state. *Phys. Rev. B* **72**, 045419. (doi:10.1103/PhysRevB.72.045419)
39 Ast, C. R., Henk, J., Ernst, A., Moreschini, L., Falub, M. C., Pacile, D., Bruno, P., Kern, K. & Grioni, M. 2007 Giant spin splitting through surface alloying. *Phys. Rev. Lett.* **98**, 186807. (doi:10.1103/PhysRevLett.98.186807)
40 Elliott, J. F., Legvold, S. & Spedding, F. H. 1953 Some magnetic properties of gadolinium metal. *Phys. Rev.* **91**, 28–30. (doi:10.1103/PhysRev.91.28)
41 Engel, H.-A., Rashba, E. I. & Halperin, B. I. 2007 Out-of-plane spin polarization from in-plane electric and magnetic fields. *Phys. Rev. Lett.* **98**, 036602. (doi:10.1103/PhysRevLett.98.036602)
42 Krupin, O., Bihlmayer, G., Doebrich, K. M., Prieto, J. E., Starke, K., Gorovikov, S., Bluegel, S., Kevan, S. & Kaindl, G. 2009 Rashba effect at the surfaces of rare-earth metals and their monoxides. *New J. Phys.* **11**, 013035. (doi:10.1088/1367-2630/11/1/013035)

43 Saarikoski, H. & Bauer, G. E. W. 2009 Spin accumulation with spin–orbit interaction. *Phys. Rev. Lett.* **102**, 097204. (doi:10.1103/PhysRevLett.102.097204)

44 Sakamoto, K. *et al.* 2009 Abrupt rotation of the Rashba spin to the direction perpendicular to the surface. *Phys. Rev. Lett.* **102**, 096805. (doi:10.1103/PhysRevLett.102.096805)

45 Stöhr, J. & Siegmann, H. C. 2006 *Magnetism, from fundamentals to nanoscale dynamics.* Berlin, Germany: Springer.

46 Mugarza, A. *et al.* 2002 Lateral quantum wells at vicinal Au(111) studied with angle-resolved photoemission. *Phys. Rev. B* **66**, 245419. (doi:10.1103/PhysRevB.66.245419)

47 Petersen, L. & Hedegard, P. 2000 A simple tight-binding model of spin–orbit splitting of sp-derived surface states. *Surf. Sci.* **459**, 49–56. (doi:10.1016/S0039-6028(00)00441-6)

48 McGuire, T. & Potter, R. 1975 Anisotropic magnetoresistance in ferromagnetic 3d alloys. *IEEE Trans. Magn.* **11**, 1018–1038. (doi:10.1109/TMAG.1975.1058782)

49 Crépieux, A. & Bruno, P. 2001 Theory of the anomalous Hall effect from the Kubo formula and the Dirac equation. *Phys. Rev. B* **64**, 014416. (doi:10.1103/PhysRevB.64.014416)

50 Nagaosa, N., Sinova, J., Onoda, S., MacDonald, A. H. & Ong, N. P. 2009 Anomalous Hall effect. (http://arxiv.org/abs/0904.4154)

51 Kato, Y. K., Myers, R. C., Gossard, A. C. & Awschalom, D. D. 2004 Current-induced spin polarization in strained semiconductors. *Phys. Rev. Lett.* **93**, 176601. (doi:10.1103/PhysRevLett.93.176601)

52 Sinova, J., Culcer, D., Niu, Q., Sinitsyn, N. A., Jungwirth, T. & MacDonald, A. H. 2004 Universal intrinsic spin Hall effect. *Phys. Rev. Lett.* **92**, 126603. (doi:10.1103/PhysRevLett.92.126603)

53 Edelstein, V. M. 1990 Spin polarization of conduction electrons induced by electric current in two-dimensional asymmetric electron systems. *Solid State Commun.* **73**, 233–235. (doi:10.1016/0038-1098(90)90963-C)

54 Chaplik, A. V., Entin, M. V. & Magarill, L. I. 2002 Spin orientation of electrons by lateral electric field in 2D system without inversion symmetry. *Physica E* **13**, 744–747. (doi:10.1016/S1386-9477(02)00273-4)

55 Inoue, J.-i., Bauer, G. E. W. & Molenkamp, L. W. 2003 Diffuse transport and spin accumulation in a Rashba two-dimensional electron gas. *Phys. Rev. B* **67**, 033104. (doi:10.1103/PhysRevB.67.033104)

56 Stern, N. P., Ghosh, S., Xiang, G., Zhu, M., Samarth, N. & Awschalom, D. D. 2006 Current-induced polarization and the spin Hall effect at room temperature. *Phys. Rev. Lett.* **97**, 126603. (doi:10.1103/PhysRevLett.97.126603)

57 Silov, A. Y., Blajnov, P. A., Wolter, J. H., Hey, R., Ploog, K. H. & Averkiev, N. S. 2004 Current-induced spin polarization at a single heterojunction. *Appl. Phys. Lett.* **85**, 5929–5931. (doi:10.1063/1.1833565)

58 Ganichev, S., Danilov, S., Schneider, P., Bel'kov, V., Golub, L., Wegseheider, W., Weiss, D. & Prettl, W. 2006 Electric current-induced spin orientation in quantum well structures. *J. Magn. Magn. Mater.* **300**, 127–131. (doi:10.1016/j.jmmm.2005.10.048)

59 Obata, K. & Tatara, G. 2008 Current-induced domain wall motion in Rashba spin–orbit system. *Phys. Rev. B* **77**, 214429. (doi:10.1103/PhysRevB.77.214429)

60 Silsbee, R. H. 2001 Theory of the detection of current-induced spin polarization in a two-dimensional electron gas. *Phys. Rev. B* **63**, 155305. (doi:10.1103/PhysRevB.63.155305)

61 Ziman, J. M. 1972 *Principles of the theory of solids.* Cambridge, UK: Cambridge University Press.

62 Datta, S. & Das, B. 1990 Electronic analog of the electro-optic modulator. *Appl. Phys. Lett.* **56**, 665–667. (doi:10.1063/1.102730)

63 Hammar, P. R. & Johnson, M. 2000 Potentiometric measurements of the spin-split subbands in a two-dimensional electron gas. *Phys. Rev. B* **61**, 7207–7210. (doi:10.1103/PhysRevB.61.7207)

64 Ngo, A. T., Villas-Bôas, J. M. & Ulloa, S. E. 2008 Spin polarization control via magnetic barriers and spin–orbit effects. *Phys. Rev. B* **78**, 245310. (doi:10.1103/PhysRevB.78.245310)

65 Matos-Abiague, A. & Fabian, J. 2009 Anisotropic tunneling magnetoresistance and tunneling anisotropic magnetoresistance: spin–orbit coupling in magnetic tunnel junctions. *Phys. Rev. B* **79**, 155303. (doi:10.1103/PhysRevB.79.155303)

66 Matos-Abiague, A., Gmitra, M. & Fabian, J. 2009 Angular dependence of the tunneling anisotropic magnetoresistance in magnetic tunnel junctions. *Phys. Rev. B* **80**, 045312. (doi:10.1103/PhysRevB.80.045312)
67 Adagideli, I., Bauer, G. E. W. & Halperin, B. I. 2006 Detection of current-induced spins by ferromagnetic contacts. *Phys. Rev. Lett.* **97**, 256601. (doi:10.1103/PhysRevLett.97.256601)
68 Pareek, T. P. & Jayannavar, A. M. 2008 Generation and measurement of nonequilibrium spin currents in two-terminal systems. *Phys. Rev. B* **77**, 153307. (doi:10.1103/PhysRevB.77.153307)
69 Yang, W., Chang, K., Wu, X. G., Zheng, H. Z. & Peeters, F. M. 2006 Interplay between s–d exchange interaction and Rashba effect: spin-polarized transport. *Appl. Phys. Lett.* **89**, 132112. (doi:10.1063/1.2357888)
70 Zhang, S. & Li, Z. 2004 Roles of nonequilibrium conduction electrons on the magnetization dynamics of ferromagnets. *Phys. Rev. Lett.* **93**, 127204. (doi:10.1103/PhysRevLett.93.127204)
71 Garate, I. & MacDonald, A. H. 2009 Influence of a transport current on magnetic anisotropy in gyrotropic ferromagnets. *Phys. Rev. B* **80**, 134403. (doi:10.1103/PhysRevB.80.134403)
72 Thiaville, A., Nakatani, Y., Miltat, J. & Suzuki, Y. 2005 Micromagnetic understanding of current-driven domain wall motion in patterned nanowires. *Europhys. Lett.* **69**, 990. (doi:10.1209/epl/i2004-10452-6)
73 Beach, G. S. D., Nistor, C., Knutson, C., Tsoi, M. & Erskine, J. L. 2005 Dynamics of field-driven domain-wall propagation in ferromagnetic nanowires. *Nat. Mater.* **4**, 741–744. (doi:10.1038/nmat1477)
74 Hayashi, M., Thomas, L., Bazaliy, Y. B., Rettner, C., Moriya, R., Jiang, X. & Parkin, S. S. P. 2006 Influence of current on field-driven domain wall motion in permalloy nanowires from time resolved measurements of anisotropic magnetoresistance. *Phys. Rev. Lett.* **96**, 197207. (doi:10.1103/PhysRevLett.96.197207)
75 Lepadatu, S., Hickey, M. C., Potenza, A., Marchetto, H., Charlton, T. R., Langridge, S., Dhesi, S. S. & Marrows, C. H. 2009 Experimental determination of spin-transfer torque nonadiabaticity parameter and spin polarization in permalloy. *Phys. Rev. B* **79**, 094402. (doi:10.1103/PhysRevB.79.094402)
76 Miron, I. M., Zermatten, P. J., Gaudin, G., Auffret, S., Rodmacq, B. & Schuhl, A. 2009 Domain wall spin torquemeter. *Phys. Rev. Lett.* **102**, 137202. (doi:10.1103/PhysRevLett.102.137202)
77 Tsoi, M., Jansen, A. G. M., Bass, J., Chiang, W.-C., Seck, M., Tsoi, V. & Wyder, P. 1998 Excitation of a magnetic multilayer by an electric current. *Phys. Rev. Lett.* **80**, 4281–4284. (doi:10.1103/PhysRevLett.80.4281)
78 Kiselev, S. I., Sankey, J. C., Krivorotov, I. N., Emley, N. C., Schoelkopf, R. J., Buhrman, R. A. & Ralph, D. C. 2003 Microwave oscillations of a nanomagnet driven by a spin-polarized current. *Nature* **425**, 380–383. (doi:10.1038/nature01967)
79 Yamanouchi, M., Chiba, D., Matsukura, F. & Ohno, H. 2004 Current-induced domain-wall switching in a ferromagnetic semiconductor structure. *Nature* **428**, 539–542. (doi:10.1038/nature02441)
80 Nicolay, G., Reinert, F., Hüfner, S. & Blaha, P. 2001 Spin–orbit splitting of the L-gap surface state on Au(111) and Ag(111). *Phys. Rev. B* **65**, 033407. (doi:10.1103/PhysRevB.65.033407)
81 Henk, J., Hoesch, M., Osterwalder, J., Ernst, A. & Bruno, P. 2004 Spin–orbit coupling in the L-gap surface states of Au(111): spin-resolved photoemission experiments and first-principles calculations. *J. Phys. Condens. Matter* **16**, 7581–7597. (doi:10.1088/0953-8984/16/43/002)
82 Rotenberg, E. & Kevan, S. 1998 Evolution of Fermi level crossings versus H coverage on W(110). *Phys. Rev. Lett.* **80**, 2905–2908. (doi:10.1103/PhysRevLett.80.2905)
83 Koroteev, Y., Bihlmayer, G., Gayone, J., Chulkov, E., Blugel, S., Echenique, P. & Hofmann, P. 2004 Strong spin–orbit splitting on Bi surfaces. *Phys. Rev. Lett.* **93**, 046403. (doi:10.1103/PhysRevLett.93.046403)
84 Rotenberg, E., Chung, J. & Kevan, S. 1999 Spin-orbit coupling induced surface band splitting in Li/W(110) and Li/Mo(110). *Phys. Rev. Lett.* **82**, 4066–4069. (doi:10.1103/PhysRevLett.82.4066)
85 Bentmann, H., Forster, F., Bihlmayer, G., Chulkov, E. V., Moreschini, L., Grioni, M. & Reinert, F. 2009 Origin and manipulation of the Rashba splitting in surface alloys. *Europhys. Lett.* **87**, 37003. (doi:10.1209/0295-5075/87/37003)

86 Rodmacq, B., Manchon, A., Ducruet, C., Auffret, S. & Dieny, B. 2009 Influence of thermal annealing on the perpendicular magnetic anisotropy of Pt/Co/AlOx trilayers. *Phys. Rev. B* **79**, 024423. (doi:10.1103/PhysRevB.79.024423)

87 Manchon, A. *et al.* 2008 X-ray analysis of the magnetic influence of oxygen in Pt/Co/AlO_x trilayers. *J. Appl. Phys.* **103**, 07A912. (doi:10.1063/1.2829896)

88 Gambardella, P. *et al.* 2003 Giant magnetic anisotropy of single Co atoms and nanoparticles. *Science* **300**, 1130–1133. (doi:10.1126/science.1082857)

89 Gambardella, P. 2003 Magnetism in monatomic metal wires. *J. Phys. Condens. Matter* **15**, S2533. (doi:10.1088/0953-8984/15/34/305)

90 Vindigni, A., Rettori, A., Pini, M. G., Carbone, C. & Gambardella, P. 2006 Finite-sized Heisenberg chains and magnetism of one-dimensional metals systems. *Appl. Phys. A* **82**, 385–394. (doi:10.1007/s00339-005-3364-4)

91 Pi, U. H., Kim, K. W., Bae, J. Y., Lee, S. C., Cho, Y. J., Kim, K. S. & Seo, S. 2010 Tilting of the spin orientation induced by Rashba effect in ferromagnetic metal layer. *Appl. Phys. Lett.* **97**, 162507. (doi:10.1063/1.3502596)

92 Miron, I. M., Garello, K., Gaudin, G., Auffret, S., Rodmacq, B., Schuhl, A. & Gambardella, P. In preparation.

93 Gierz, I. *et al.* 2009 Silicon surface with giant spin splitting. *Phys. Rev. Lett.* **103**, 046803. (doi:10.1103/PhysRevLett.103.046803)

94 Koitzsch, C., Battaglia, C., Clerc, F., Despont, L., Garnier, M. G. & Aebi, P. 2005 Photoemission of a quantum cavity with a nonmagnetic spin separator. *Phys. Rev. Lett.* **95**, 126401. (doi:10.1103/PhysRevLett.95.126401)

95 Frantzeskakis, E., Pons, S., Mirhosseini, H., Henk, J., Ast, C. R. & Grioni, M. 2008 Tunable spin gaps in a quantum-confined geometry. *Phys. Rev. Lett.* **101**, 196805. (doi:10.1103/PhysRevLett.101.196805)

96 Varykhalov, A., Sánchez-Barriga, J., Shikin, A. M., Gudat, W., Eberhardt, W. & Rader, O. 2008 Quantum cavity for spin due to spin–orbit interaction at a metal boundary. *Phys. Rev. Lett.* **101**, 256601. (doi:10.1103/PhysRevLett.101.256601)

97 Dil, J. H., Meier, F., Lobo-Checa, J., Patthey, L., Bihlmayer, G. & Osterwalder, J. 2008 Rashba-type spin–orbit splitting of quantum well states in ultrathin Pb films. *Phys. Rev. Lett.* **101**, 266802. (doi:10.1103/PhysRevLett.101.266802)

98 Gamble, S. J., Burkhardt, M. H., Kashuba, A., Allenspach, R., Parkin, S. S. P., Siegmann, H. C. & Stöhr, J. 2009 Electric field induced magnetic anisotropy in a ferromagnet. *Phys. Rev. Lett.* **102**, 217201. (doi:10.1103/PhysRevLett.102.217201)

99 Gould, C., Rüster, C., Jungwirth, T., Girgis, E., Schott, G. M., Giraud, R., Brunner, K., Schmidt, G. & Molenkamp, L. W. 2004 Tunneling anisotropic magnetoresistance: a spin-valve-like tunnel magnetoresistance using a single magnetic layer. *Phys. Rev. Lett.* **93**, 117203. (doi:10.1103/PhysRevLett.93.117203)

100 Gao, L., Jiang, X., Yang, S.-H., Burton, J. D., Tsymbal, E. Y. & Parkin, S. S. P. 2007 Bias voltage dependence of tunneling anisotropic magnetoresistance in magnetic tunnel junctions with MgO and Al_2O_3 tunnel barriers. *Phys. Rev. Lett.* **99**, 226602. (doi:10.1103/PhysRevLett.99.226602)

101 Park, B. G., Wunderlich, J., Williams, D. A., Joo, S. J., Jung, K. Y., Shin, K. H., Olejník, K., Shick, A. B. & Jungwirth, T. 2008 Tunneling anisotropic magnetoresistance in multilayer-(Co/Pt)/AlO_x/Pt structures. *Phys. Rev. Lett.* **100**, 087204. (doi:10.1103/PhysRevLett.100.087204)

102 Chantis, A. N., Belashchenko, K. D., Tsymbal, E. Y. & van Schilfgaarde, M. 2007 Tunneling anisotropic magnetoresistance driven by resonant surface states: first-principles calculations on an Fe(001) surface. *Phys. Rev. Lett.* **98**, 046601. (doi:10.1103/PhysRevLett.98.046601)

103 Khan, M. N., Henk, J. & Bruno, P. 2008 Anisotropic magnetoresistance in Fe/MgO/Fe tunnel junctions. *J. Phys. Condens. Matter* **20**, 155208. (doi:10.1088/0953-8984/20/15/155208)

104 Wimmer, M., Lobenhofer, M., Moser, J., Matos-Abiague, A., Schuh, D., Wegscheider, W., Fabian, J., Richter, K. & Weiss, D. 2009 Orbital effects on tunneling anisotropic magnetoresistance in Fe/GaAs/Au junctions. *Phys. Rev. B* **80**, 121301. (doi:10.1103/PhysRevB.80.121301)